Journal of Laser Applications ARTICLE scitation.org/journal/jla

CO_2 laser-assisted sintering of TiO_2 nanoparticles for transparent films

Cite as: J. Laser Appl. 35, 012012 (2023); doi: 10.2351/7.0000821
Submitted: 8 July 2022 · Accepted: 8 December 2022 ·
Published Online: 3 January 2023

Yahya Bougdid,[1] Francois Chenard,[2] John Sugrim,[3] Ranganathan Kumar,[4] and Aravinda Kar[1,a)]

AFFILIATIONS

[1]Center for Research and Education in Optics and Lasers (CREOL), The College of Optics and Photonics, University of Central Florida, Orlando, Florida 32816
[2]IRflex Corporation, 300 Ringgold Industrial Parkway, Danville, Virginia 24540
[3]Navy Jacksonville Florida, Jacksonville, Florida 32092
[4]Department of Mechanical and Aerospace Engineering, University of Central Florida, Orlando, Florida 32816

Note: This paper is part of the Special Collection: Laser Additive Manufacturing Processes: From Cladding to Complex Parts.
[a)]**Electronic mail:** akar@creol.ucf.edu

ABSTRACT

Nanoelectrospray laser deposition (NELD) of nanoparticles (NPs) on various substrates has attracted considerable attention as a fast, cost-effective, and scalable technique for precise control of heating time and zone. In this work, NELD-assisted sintering of titanium dioxide (TiO_2) NPs on borosilicate glass and quartz substrates is addressed. A 10.6 μm CO_2 laser was used for patterning and sintering titania nanoparticles in ambient air. The effects of laser dose and deposition process parameters on the morphological, structural, and optical characteristics of the sintered TiO_2 patterns were characterized using optical microscopy, scanning electron microscopy, and x-ray diffraction. The results point out that the anatase phase was preserved after laser sintering, without the appearance of any TiO_2 rutile traces. We show that the improvement in the morphological properties of TiO_2 patterns is due to the laser sintering of a dense layer of ceramic with enhanced interconnectivity and connection between single nanoparticles. A theoretical model was developed to select the temperature required to sinter TiO_2 nanoparticles and to correlate it with the laser power and scanning speed to prevent cracking on the substrate and sintered nanoparticles and also to get transparent TiO_2 films. An optical transmittance of ~91% was achieved. The experimental data were in accordance with the theoretical model, predicting the success of the model.

I. INTRODUCTION

Nanoparticles (1–100 nm in size), i.e., the building blocks for nanotechnology, are the raw nanomaterial for manufacturing microdevices for a broad spectrum of applications.[1,2] Particle transport through Marangoni convection inside a sessile droplet can be controlled by the ultraviolet light distribution on the surface for selective area deposition of nanoparticles.[3–5] Localized laser printing and sintering of silver nanoparticles (NPs) for silicon solar cell metallization have been performed using a laser-assisted electrospray deposition method[6] and the effect of laser power on the conductivity and morphology of silver nanoparticle thin films has been determined.[7] Recently, due to the emergence of a new generation of high-technology materials, titanium dioxide (TiO_2) has been under extensive investigation due to its advanced applications as and its excellent and unique properties, such as wide bandgap, chemical stability, and high transmittance combined with a high refractive index.[8] TiO_2 is a wide bandgap nanomaterial and has crucial applications in the coating of optical lenses.[9] TiO_2 exists in three crystalline forms; i.e., anatase, rutile, and brookite.[10] Rutile is the most stable phase of TiO_2 under ambient conditions and has a high refractive index which makes it suitable for protective coatings on lenses;[9] also in optoelectronic, both crystalline rutile and anatase are applied.[11] Yu *et al.*[12] investigated that anatase can be utilized for photocatalysis due to its fast response to UV light. Liu *et al.*[13] reported that amorphous TiO_2 can be applied in biomedicine due to its blood compatibility. Controlling the phase transformation of TiO_2 from amorphous to crystalline forms is an important challenge because the micro-architecture of TiO_2

influences the deposited film properties.[8,11] Mathews *et al.*[14] confirmed by using x-ray diffraction that the anatase phase is formed close to a temperature of ~400 °C. Nagpal *et al.*[15] showed that at 500 °C, TiO_2 is still amorphous and the anatase phase began around ~600 °C, and the TiO_2 film turned opaque at 800 °C due to the densification of TiO_2 nanoparticles. Therefore, the change of TiO_2 phases strongly depends on the chemical composition, temperature, and size of the particles.

In additive manufacturing, the processing of a solgel film by laser is a straightforward and efficient tool and has several advantages compared to conventional techniques of annealing in a furnace. Lasers with different wavelengths have been applied for thermal processing.[8,10] Schade *et al.*[16] investigated the effect of power on TiO_2 particles size using a UV laser of $\lambda = 193$ nm. Yang *et al.*[8] reported the 355 and 1064 nm laser sintering of TiO_2 on a plastic substrate for highly efficient, flexible, dye-sensitized solar cell applications. In this context, the above-reported studies used thin-film deposition followed by an annealing step, but it is difficult to directly deposit nanoparticles into large 2D or 3D patterns, such as discrete arrays and periodic microstructures. The most common conventional technique incorporates various steps, such as thin-film deposition using spin-coating, light irradiation, and also including etching and developing steps.[11,13,14] These methods take into account a separate postdeposition annealing step and, in addition, may require physical contact, which can increase the cross contamination issue. The annealing step can be a problem for substrates with a low melting point.[1,8]

Laser-microdroplet interactions influence the quality of nanoparticle deposition on a substrate. In this research, we show an efficient technique to deposit and sinter TiO_2 nanoparticles known as the NELD (nanoelectrospray laser deposition) process, where a laser beam can be used to evaporate the organic solvent and simultaneously sinter the nanoparticles at desired locations on different substrates[1,17–20] or in mid-air.[21] In comparison to the traditional methods, NELD offers a fast, cost-effective, and scalable method for sintering and patterning micro- and nano-structures. Also, few expensive techniques have been developed for microscale laser printing, e.g., two-photon nanolithography.[22,23] An attractive advantage of using CO_2 laser is that the sintering temperature of titania nanoparticles has been observed to be less than the melting temperature of the substrate; this special propriety leads to a reduction in cost and enables applicability to a large area of printing. NELD strategy shows several advantages: (1) TiO_2 patterns can be sintered with a faster processing speed, (2) NELD allows localized sintering of nanoparticles around the micro-focused laser spot without heating the surrounding of the substrate, and (3) there is no damage on the substrates due to low heat input.[17,18] The NELD process has many advantages for our study, such as controllable TiO_2 phase, low cost, printing of desired patterns, and ease of operation in the air. Therefore, we have used the NELD process for depositing and sintering TiO_2 nanoparticles (anatase and amorphous) on borosilicate glass and quartz substrates for transparent films, and its applications in coating optical lenses. We study the effects of different process parameters on the morphological, structural, and optical properties of the printed TiO_2 patterns. A theoretical model is developed to select proper process parameters to minimize the number of experiments and produce transparent TiO_2 films. Several experiments, e.g., drop casting, are performed using different optimized parameters to adjust the thickness of transparent TiO_2 films that can be used in advanced optics applications.

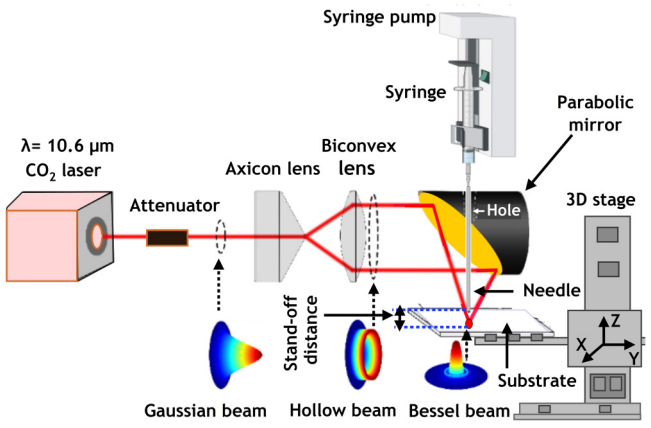

FIG. 1. Schematic of the experimental setup for depositing and sintering TiO_2 NPs using the NELD process.

II. EXPERIMENTAL PROCEDURE

A. NELD process

Figure 1 illustrates the NELD setup used for the laser deposition of TiO_2 nanoparticles. The TiO_2 suspension can be deposited and sintered on the substrate around the vicinity of the defocused laser spot. The basics of the NELD process have been discussed previously.[1,17] In this work, we used two types of materials: (1) 99.99%, anatase TiO_2 nanoparticles (50 wt. % , particles size: 18 nm) in ethylene glycol (EG), and (2) 99.9%, amorphous:anatase = 4:1 TiO_2 nanoparticles (50 wt. % , particles size: 5 nm) in EG. Prior to deposition, the nanosuspensions were ultrasonicated for 20 min at 80 MHz frequency, and the resulting suspensions were used to deposit TiO_2 patterns. Before deposition, the substrates were cleaned using an ultrasonic cleaner with three stages in which we used acetone, methanol, and de-ionized water, respectively. Two types of substrates, borosilicate glass and fused quartz glass, have been used in this study because borosilicate glass has a higher coefficient of thermal expansion ($\sim 5 \times 10^{-6}$/°C at 20 °C), lower melting onset temperature (560 °C), and lower spectral range (0.3 −2.5 μm) for light transmission than the respective properties ($\sim 5.5 \times 10^{-7}$/°C at 20 °C, 1900 °C and 0.16 − 3.5 μm) of fused silica. The lower thermal expansion coefficient of fused quartz makes it more resistant to thermal shock and, therefore, less prone to cracking during the laser-assisted deposition of transparent TiO_2 thin films on fused quartz than on borosilicate substrates. In spite of this difference in the thermal shock resistance, this study demonstrates deposition without cracking both types of substrates. With regard to the other two properties, a higher melting onset temperature and a higher spectral transmission range of fused quartz suggest that TiO_2-coated fused quartz can be used as an optical window at high temperatures over a large spectral range.

TABLE I. Properties of TiO_2 NPs, EG, and TiO_2 nanoparticles + EG.

	TiO_2 NPs	EG	NPs + EG
Thermal conductivity [W/(m K)]	8.4	0.258	4.329
Thermal diffusivity (10^{-6} m^2/s)	5.06	0.11	2.58
Absorbance (%)	55	97	76

TiO_2 suspension was delivered to the laser-substrate interaction zone using a capillary tube or a needle of 838 μm inner diameter (ID). A controlled syringe pump was used to push the plunger in a syringe for delivering the nanoparticles onto the substrate. The deposited nanoparticles interact with the CO_2 laser operated at a continuous wave mode. The original Gaussian beam from the laser source is converted into an annular beam of nearly uniform radial irradiance distribution through a ZnSe axicon lens and a biconvex lens, respectively, and the annular beam is focused with a parabolic mirror to form a hollow laser cone. At the focal point of the parabolic mirror, i.e., the apex of the cone, the original Gaussian beam transformed to a Gauss–Bessel beam with an irradiance distribution different from the typical Gaussian irradiance distribution. The defocused laser spot is set at ~1 mm diameter. The laser beam was defocused from 300 nm (original size of the apex of the cone) to 1 mm to avoid cracking on the glass substrate. The syringe pump was set up above the parabolic mirror so that the capillary tube could be placed in a coaxial configuration, where it was passed through the hole inside the parabolic mirror, as shown in Fig. 1. The interaction among the laser, TiO_2 nanoparticles, and substrate occurs at the apex of this cone, and the interaction process is controlled to deposit TiO_2 nanoparticles in two steps: drying of the suspension and sintering of TiO_2 nanoparticles. The substrate is moved beneath the laser beam by operating the 3D stage. The 3D stage we used is 150 mm Linear Translation Stage, Stepper Motor, Thorlabs. A high-power detector, 818P-250-25 Series, Newport, was used to measure the CO_2 laser power.

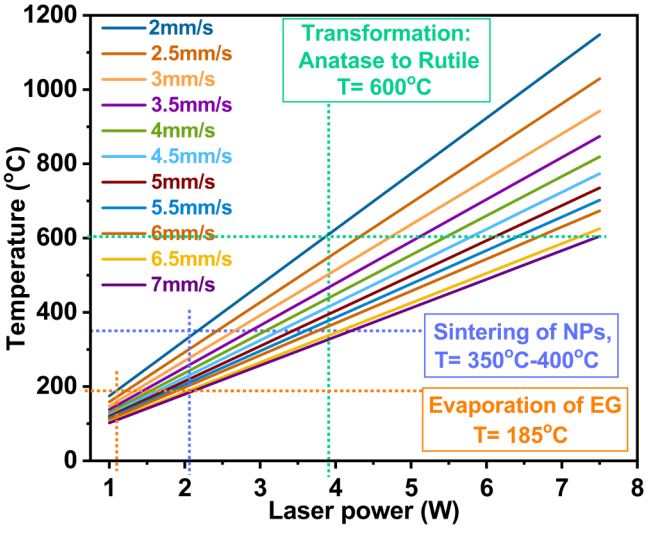

FIG. 2. Calculated temperature as a function of laser power for different substrate speeds.

B. Characterization

The characterization of samples was carried out using an optical microscope (Nikon, Japan), Zeiss ULTRA-55 FEG SEM (scanning electron microscopy), XRD Basic Diffraction PANalytical Empyrean (x-ray diffraction), and an Agilent Cary 5000 UV-VIS-NIR spectrophotometer. Before SEM measurements, samples were coated with a 1 nm layer of gold in order to prevent the charging effects during the interaction of electrons with the samples' surfaces.

III. PROCESS PARAMETERS SELECTION

In this work, we investigated how TiO_2 nanoparticles could be deposited and sintered using the NELD process. Generally, laser deposition of nanoparticles requires a proper choice of all processing parameters aiming to trigger efficient sintering and minimize substrate damage and material loss. By using the mixture rule, we calculated the properties of TiO_2 suspension (i.e., TiO_2 NPs dispersed in EG). Table I presents the thermal and optical properties of TiO_2, EG, and the mixture. CO_2 laser deposition of TiO_2 nanoparticles is carried out in two steps: (1) preheating and (2) sintering. However, to prevent the loss of TiO_2 nanomaterial during the drying step, we selected appropriate process parameters corresponding to the temperature required to evaporate EG. First, we calculated the absorbance of EG by determining the reflectance value (R) using the following formula:

$$R = \frac{(n-1)^2 + k^2}{(n+1)^2 + k'}, \tag{1}$$

where n is the refractive index of EG and k is a constant ($k = 0.000\,121$, negligible). The reflectance of EG at 10.6 μm is found to be around 0.0326; thus, the absorbance is ~ 97% ($A = 1 - R$).[24]

Hence, the laser power and scanning speed needed to evaporate EG can be calculated to be 1.1 W and 2 mm/s, respectively. The sintering of TiO_2 nanoparticles using CO_2 laser has not been widely reported.[8,16] The NELD process allows for variable widths and heights of TiO_2 patterns. Once the TiO_2 patterns are deposited, CO_2 laser sintering can take place.

Understanding the proper temperature based on other parameters is important for the proper sintering of nanoparticles. The sintering temperature is estimated to be the temperature[25,26] on the surface at the laser-material interaction zone at any time t during the irradiation of this interaction zone by the laser beam,

$$T(0, t) = T_r + \left(\frac{2AP}{ka}\right)\left(\frac{\alpha t}{\pi}\right)^{1/2}. \tag{2}$$

Here, T_r denotes the room temperature, A is the absorptivity of TiO_2 at $\lambda = 10.6\,\mu$m, k is the thermal conductivity, and α is the

thermal diffusivity. P is the power, and a is the area of interaction between the laser and TiO_2 nanoparticles. The area where titania nanoparticles are deposited, $T(0, t_{int})$ is obtained from Eq. (2) at the laser-material interaction time $t = t_{int} = d/v$, where d is the laser diameter and v is the substrate speed. Using the model in Eq. (2), the temperature is calculated as a function of laser power for different substrate speeds, as shown in Fig. 2.

Figure 3 shows the heating rate; i.e., the rate at which the temperature is raised per unit of time, as a function of laser power for different scanning speeds. The derivative of temperature with respect to time; i.e., $dT(0, t)/dt$, gives the rate of heating. Starting from Eq. (2), the derivative is determined and then the heating rate is obtained at $t = t_{int}$, as follows:

$$\frac{dT}{dt} = \left(\frac{AP}{ka}\right)\left(\frac{\alpha}{\pi}\right)^{1/2}\frac{\sqrt{v}}{\sqrt{d}}. \tag{3}$$

Equation (3) determines how fast the substrate is heating up during laser processing. Using 2 W laser power at low substrate speed minimizes the heating effect and successfully sinters the TiO_2 nanoparticles without any damage to the substrate. Based on the model (Fig. 3), a minimum laser power, combined with a low substrate speed, is required to minimize the effect of heating, thus minimizing the loss of TiO_2 material.

Equation (2) is a special case of the general temperature distribution during laser heating of the laser-material interaction zone. The general case, which represents the spatial and temporal variations of the temperature, is given by the following expression:[25,26]

$$T(z, t) = \frac{2I}{k}\left(\frac{\alpha t}{\pi}\right)^{1/2} e^{-\frac{z^2}{4\alpha t}} - \frac{Iz}{k}\, erfc\left(\frac{z}{2\sqrt{\alpha t}}\right), \tag{4}$$

where z is the vertically downward axis with origin at the center of the laser beam on the surface of the material. Taking $T(z, t_{int})$ from Eq. (4) as the initial condition, the solution of a one-dimensional transient heat conduction equation[25,26] represents the temperature distribution, $T_c(z, t)$, in the material during the cooling period when the laser beam passes out of the laser-material interaction zone. The derivative of $T_c(z, t)$ with respect to time is evaluated at $z = 0$ and $t = t_{int}$ to obtain Eq. (5). This equation expresses the cooling rate on the surface of the material at the laser-material interaction time t_{int},

$$-\frac{dT_c}{dt} = \frac{I}{k}\sqrt{\frac{\alpha}{\pi}}\,\frac{\sqrt{2}-1}{\sqrt{2}}\frac{\sqrt{v}}{\sqrt{d}};\; I = \frac{P}{a}. \tag{5}$$

Figure 4 shows the dependency of the cooling rate as a function of power for different scanning speeds. TiO_2 nanoparticles have been sintered using 2 W power at 2 mm/s speed to optimize the heating and cooling rates. The cooling rate in Fig. 4 signifies the cooling of the glass substrate along with its interaction with the laser spot, which induces the thermal energy required for the sintering of TiO_2 nanoparticles. The cooling rate is significantly low for low velocities of laser scanning combined with low power.

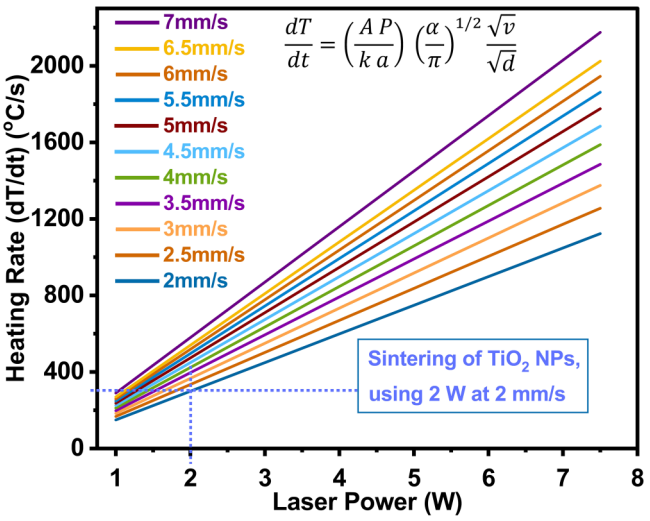

FIG. 3. Calculated heating rate as a function of laser power for different substrate speeds.

To get a slow cooling of the substrate during the laser processing, a minimum power of 2 W at a low scanning speed was chosen. To prevent the breakage of the substrate and, simultaneously, sinter the TiO_2 nanoparticles with a sufficient cooling rate, a scanning speed of 2 mm/s was chosen. The main reason for the breakage of the glass substrate is the effect of high cooling rates.

IV. RESULTS AND DISCUSSION

Different methods such as chemical vapor deposition, sputtering, and solgel have been used for depositing TiO_2 nanoparticles followed by the post furnace annealing step to control the phase transformation.[13,14,17] Thermal annealing in a furnace is the most

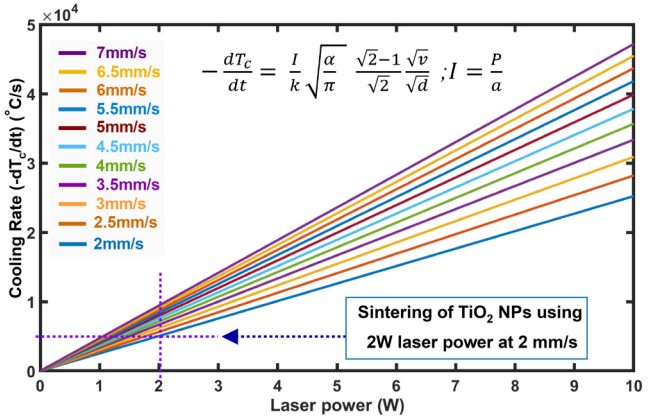

FIG. 4. Theoretical cooling rate as a function of laser power for different scanning speeds.

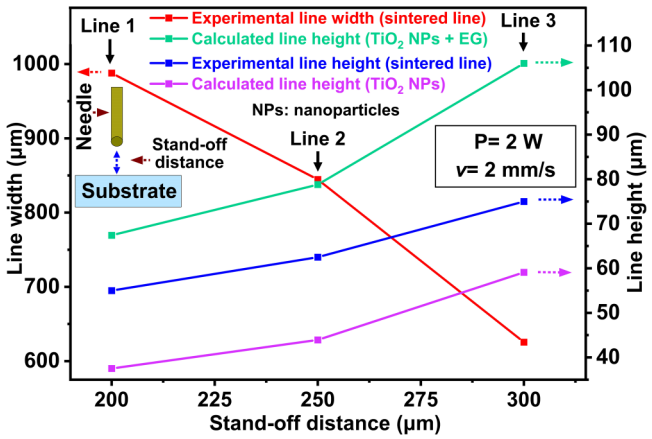

FIG. 5. Experimental and calculated data. Red: measured width of the sintered TiO_2 lines. Green: calculated line height based on nanoparticles + EG. Blue: measured height of the sintered lines. Pink: calculated height of nanoparticles-based lines, as a function of stand-off distance.

popular technique utilized for controlling TiO_2 phases, and the expensive excimer UV laser is sometimes used to produce transparent TiO_2 films.[8,16] The NELD process in the current study provides a convenient way for printing the 2D and 3D structures at a micrometric scale. Therefore, several fascinating effects can be observed when titania NPs interact with laser-assisted sintering. Based on the model developed in this study, a power of 2 W combined with 2 mm/s speed can be as the threshold for the laser dose at which the nanoparticles can be properly sintered, as they become yellow, which is the original color of anatase TiO_2. 2 W power at 2 mm/s

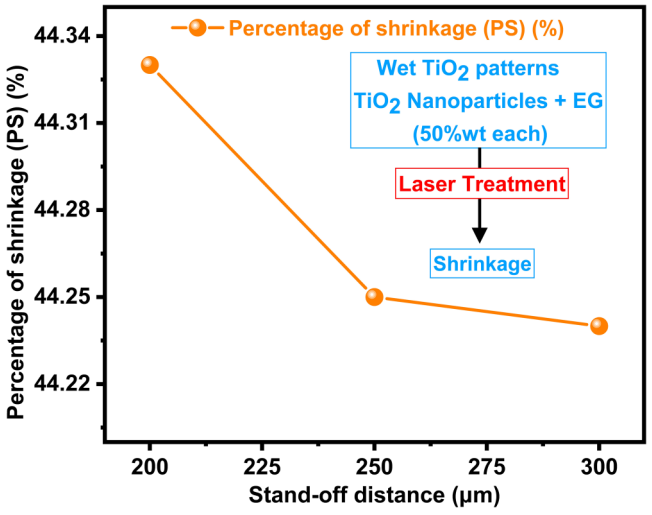

FIG. 6. Percentage shrinkage of the printed TiO_2 lines after laser treatment for different stand-off distances.

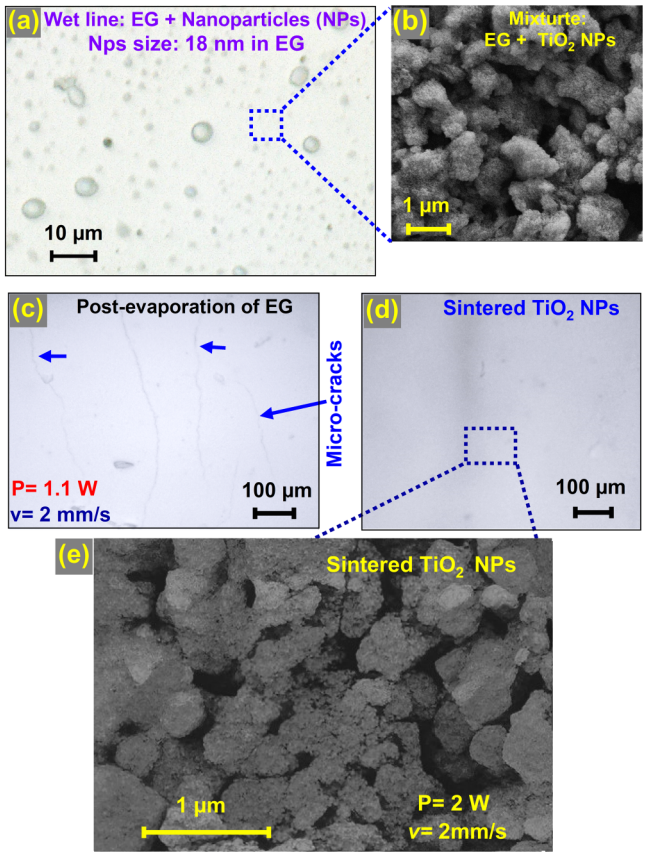

FIG. 7. Laser sintering of 99.99% anatase TiO_2. (a) Optical micrograph (2000X) of a wet line. (b) SEM image of the wet line shown in (a). (c) Optical image (100X) of TiO_2 line post evaporation of EG. (d) Optical micrograph (100X) of the sintered line. (e) SEM image showing the sintered nanoparticles in (d).

speed gives rise to a temperature of ~350 °C at the center of the laser spot according to Eq. (2). Mufti *et al.*[27] reported that the annealing of TiO_2 nanoparticles at 350 °C presents a crystalline TiO_2 anatase phase. This result was confirmed by x-ray diffraction measurements.

In the first experiment, for the sintering of 99.99% anatase TiO_2 nanoparticles (50 wt. %, particles size: 18 nm, in EG) (Fig. 7), the effect of stand-off distance on the experimental width (W) and height (H) of the sintered TiO_2 lines is determined, as presented in Fig. 5. Stand-off distance is defined as the distance between the needle tip from where the TiO_2 suspension is delivered and the substrate, as shown in Fig. 1. The flow rate and the substrate speed were maintained at 200 nL/min and 3 mm/s, respectively, for all lines. Using optical microscopy measurements, it is seen that W increases when the stand-off distance decreases, and oppositely H decreases, as shown in Fig. 5. This dependency is also influenced by the high viscosity of TiO_2 paste, which means, if the needle-substrate gap is larger than ~450 μm, the deposition would not

have been uniform, affecting the morphology of the printed TiO_2 patterns.

Experimentally, a minimum H is needed to allow the laser to penetrate along the thickness of deposited NPs in order to get efficient sintering. A stand-off distance of 200, 250, and 300 μm leads to an experimental line height of 55.0, 62.5, and 75.0 μm, respectively. Therefore, it is clear that thinner patterns can be achieved by using a short stand-off distance (Fig. 5). It was found that a minimum distance of ~200 mm is required for TiO_2 printing. To confirm the correlation between the width and height of TiO_2 lines and the deposition process parameters, the height is calculated from the experimental data. From the mass balance, the line height is calculated (Fig. 5). The mass balance is given by $\dot{m} = W \cdot H \cdot v \cdot \rho$, where $\dot{m}$ is the mass flow rate, W is the line width, v is the substrate speed, ρ is the density of the material, and H is the line height. Table II shows the measured and calculated dimensions of TiO_2 lines versus the stand-off distance.

The calculated heights for the (TiO_2 NPs + EG)-based lines are greater than the measured heights of sintered TiO_2 lines. As shown in Fig. 6, the shrinkages of TiO_2 lines after laser treatment are 44.33%, 44.25%, and 44.24% for the stand-off distance of 200, 250, and 300 μm, respectively. This decreasing trend is attributed to the laser evaporation of EG (50 wt. %) at the laser power of 1.1 W at 2 mm/s substrate speed.

The measured height of the sintered TiO_2 lines is higher than the calculated height of the original NPs by ~19 μm from Table II. This discrepancy may be due to (1) the incomplete evaporation of EG yielding residual micro- and nano-droplets of EG in the sintered lines and (2) the formation of pores during the evaporation of EG. These two mechanisms can cause residual tiny droplets or bubbles of EG inside the sintered patterns. The bubbles appear as pores in the resulting film. The difference in the measured and calculated heights may be reduced by increasing the number of laser passes to completely evaporate EG and to enhance the bonding of TiO_2 nanoparticles, or by depositing thinner TiO_2 lines. Thicker structures of the anatase TiO_2 crystalline phase can be built by depositing multiple layers of thin films on top of each other like in the additive manufacturing process.

Figure 7 presents the optical and SEM micrographs of wet, post-evaporated, and sintered TiO_2 patterns. Figure 7(a) shows an optical image of a wet line in which the TiO_2 nanoparticles are mixed with EG. It is clearly shown that the surface of the as-deposited line is rough due to the presence of EG. As confirmed by the SEM image in Fig. 7(b), the as-deposited TiO_2 line shows no interconnectivity between the nanoparticles. Before starting the sintering, the evaporation of EG plays an equally important role in achieving an efficient bonding of NPs. Shown in Fig. 7(c) is an optical image of the TiO_2 line after laser evaporation at 1.1 W. EG is evaporated, and the roughness decreased along with the appearance of micro-cracks [Fig. 7(c)]. The post-evaporated TiO_2 patterns exhibit some cracks, which is due to the evaporation of EG. After laser sintering, however, the TiO_2 patterns become smooth without any micro-cracks as shown in Fig. 7(d).

To investigate the difference in morphology between wet and sintered nanoparticles, 2 W power is used to sinter the evaporated TiO_2 lines [Figs. 7(d) and 7(e)]. After sintering, the morphology changes from the solgel form (EG + NPs mixture) to a solid and compact layer based only on sintered nanoparticles. It is seen that

TABLE II. Measured and calculated W and H as a function of stand-off distance.

Line ID	1	2	3
Stand-off distance (μm)	200	250	300
Measured width after sintering (μm)	987.9	844.6	625.6
Measured height after sintering (μm)	55.00	62.5	75.0
Calculated height (NPs + EG) (μm)	67.40	78.8	106.0
Calculated height (NPs) (μm)	37.5	43.9	59.1

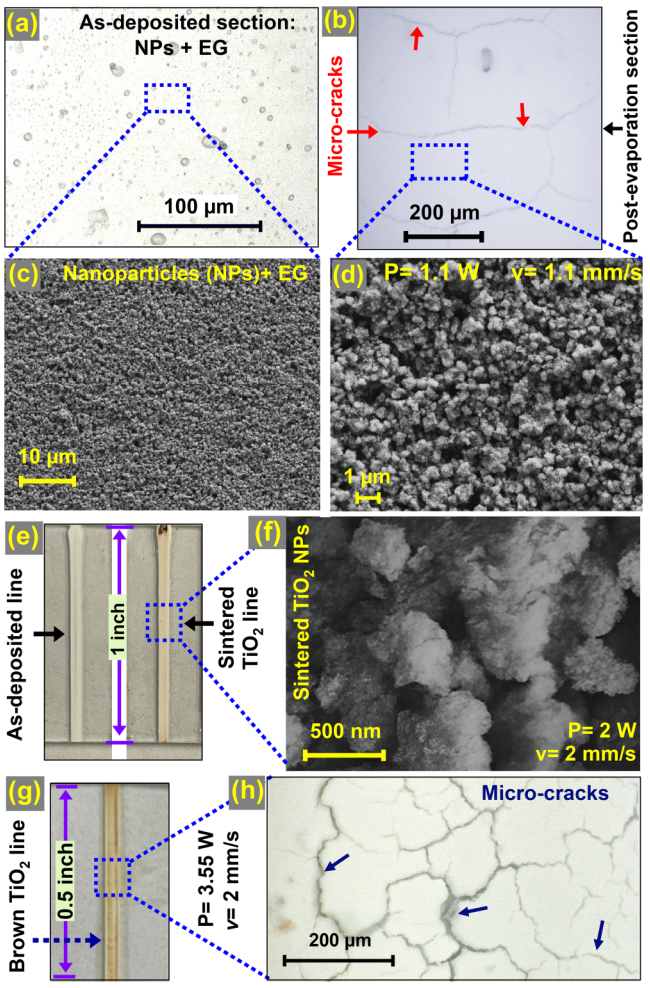

FIG. 8. Laser deposition of amorphous TiO_2. (a) Optical image (500X) of the as-deposited line. (b) Optical image (100X) of the laser evaporated line. (c) SEM image of the as-deposited section shown in (a). SEM image of the post-evaporated section shown in (b). (e) Image showing the difference in color between wet and sintered nanoparticles. (f) SEM image of sintered TiO_2 nanoparticles. (g) An image of a sintered line using a higher power (3.55 W). (h) An optical image showing the micro-cracks.

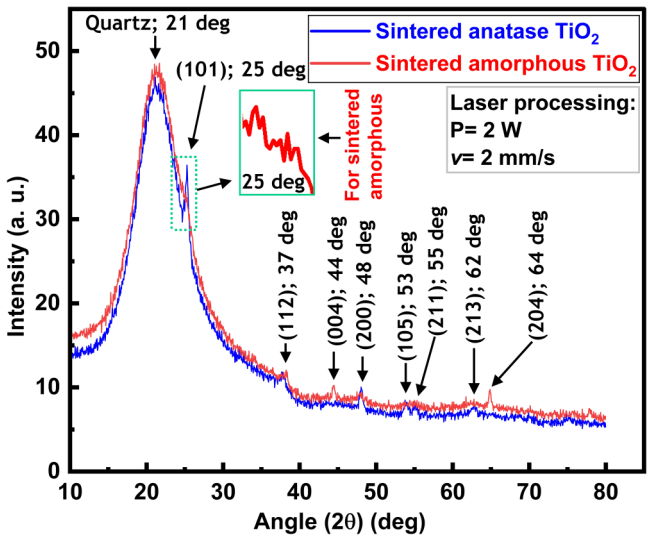

FIG. 9. X-ray diffraction of sintered anatase (blue) and sintered amorphous (red) TiO_2 films deposited on quartz substrates. The dominant blue and red peaks around $2\theta = 21°$ correspond to the substrate (Ref. 30) and all other peaks correspond to the anatase phase of TiO_2 (Refs. 31–33).

the sintering process introduces a shift in the apparent color, from a white color (wet TiO_2 lines) to a yellow color for the sintered lines. The significant change in the morphology is due to the formation of ceramic structures in a large area through the agglomeration of nanoparticles. Better adhesion of nanoparticles with each other is shown by the SEM image in Fig. 7(e). The change in

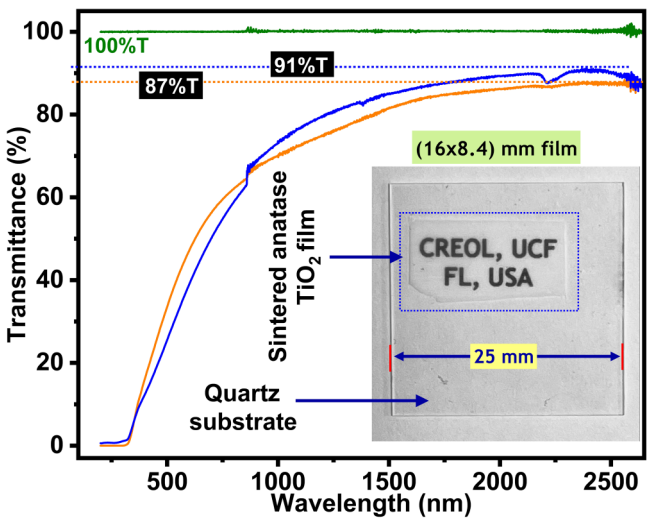

FIG. 10. Transmittance of the wet TiO_2 film (orange), sintered TiO_2 film (blue), and as a reference (green).

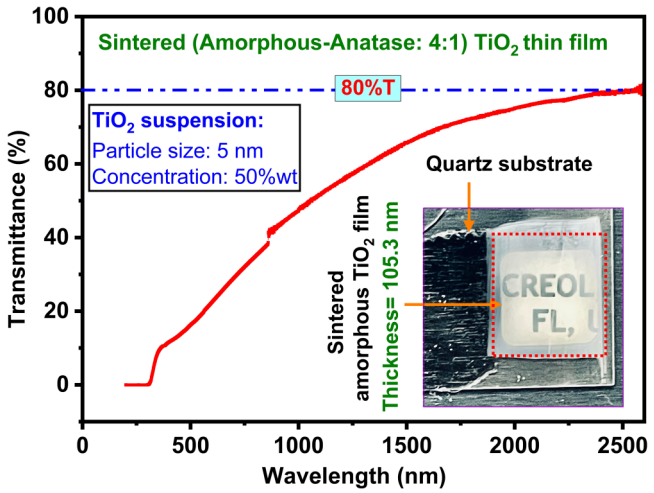

FIG. 11. Optical transmittance of sintered 4:1-amorphous:anatase TiO_2 thin films.

contrast between the unsintered and sintered TiO_2 lines is due to the microscale reorganization of porosity and surface roughness; this is caused by strong diffusion of the incident light coming from the objective microscope utilized for characterization. Radovic *et al.*[28] investigated the laser sintering of screen-printed TiO_2 nanoparticles for the improvement of mechanical proprieties. An improvement in mechanical proprieties of the sintered TiO_2 thin films was detected.[28]

The formation of necking between nanoparticles during laser sintering results in an improved mutual connectivity and a much

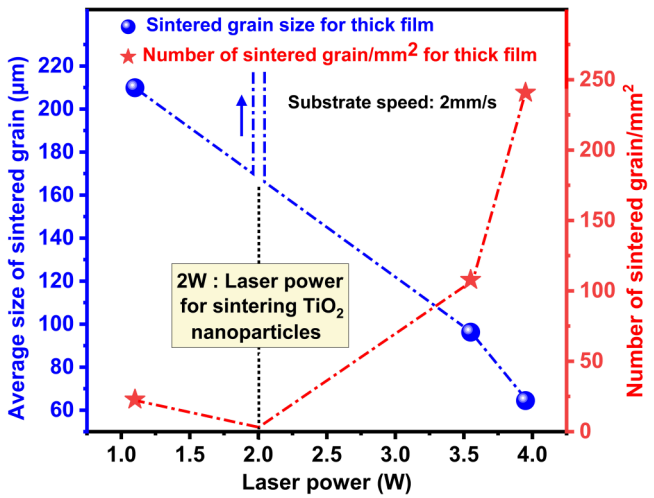

FIG. 12. Summary of the average size of sintered TiO_2-grain (blue), and the number of sintered TiO_2-grains per mm^2 (red), as a function of laser power.

TABLE III. Average size of sintered grains and the number of sintered grains per unit area for thick TiO_2 films for different laser powers.

Laser power (W)	1.1	3.55	3.95
Average size of sintered grain (μm)	209.88	96.25	64.44
Number of sintered (grain/mm^2)	22.89	107.87	240.81

smoother surface [Fig. 7(d)]. As shown in Figs. 7(d) and 7(e), a higher compactness of the sintered TiO_2 pattern can be detected. This mechanical property is accompanied by a remarkable increase in specific surface area and enhanced bonding force between the nanoparticles.[8] It was previously reported[28] that the absence of carbon in the sintered TiO_2 nanoparticles using EDX mapping confirmed the removal of organic solvent.

In the second experiment, we investigated the laser deposition of TiO_2 nanoparticles: amorphous:anatase = 4:1. Shown in Figs. 8(a)–8(d) is the effect of the laser evaporation step on the morphology of the TiO_2 patterns. It is clearly observed that the post-evaporated section [Fig. 8(b)] shows more smoothness compared to the as-deposited mixture of TiO_2 nanoparticles + EG [Fig. 8(a)]; this is due to the removal of EG. Figure 8(e) presents the difference in the color of the TiO_2 line before (white) and after laser sintering (yellow). The TiO_2 line becomes yellow as the compactness becomes high due to particle coalescence compared to the wet TiO_2 line. As the laser is focused on nanoparticles with an appropriate dose of irradiation, the optical energy is directly converted into thermal energy through a photo-thermal mechanism and triggers the sintering of titania nanoparticles with high controllability and selectivity.[8,10]

Laser treatment causes not only coalescence nanoparticles and sintering, but also phase transition from anatase to rutile[15] along with a change of color as shown in Fig. 8(e). The color change of TiO_2 is mainly due to the pairing and unpairing of electrons. Yellow color is due to oxygen defects and blue color is due to the charge transfer of $Ti^{3+} - Ti^{4+}$, while white or a colorless nature is due to the unpaired electron.[29] The yellow color is from TiO_2 anatase. The results indicate that the anatase structure after

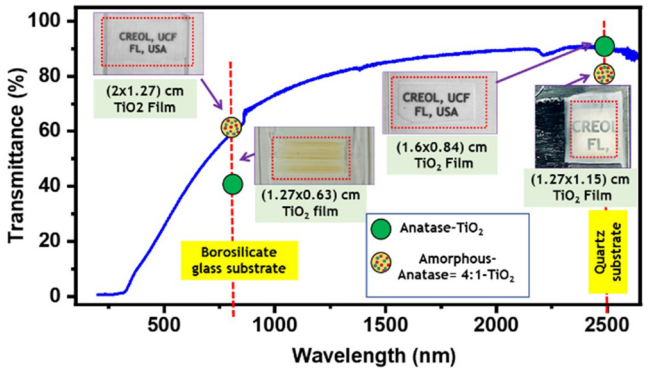

FIG. 13. Summary of the measured optical transmittance of sintered TiO_2 films.

sintering has a strong dependence on the laser processing parameters. Laser sintering at 3.55 W power and 2 mm/s speed is shown in Fig. 8(g). It is clearly seen that the TiO_2 patterns change color from white to brown due to the high laser dose. This is confirmed by the appearance of micro-cracks on the laser-treated samples, as shown in Fig. 8(h).

This study focuses on pure anatase TiO_2, unlike in most previous reported studies, where the TiO_2 mixture used for investigation is composed of two phases; e.g., 80 wt. % anatase and 20 wt. % rutile.[10,27] To understand the behavior of TiO_2 phases, XRD analysis (Fig. 9) was carried out to investigate the crystalline form of the sintered anatase and amorphous TiO_2 films (371.9 nm thickness).

The sintered TiO_2 films prepared using both anatase and amorphous titania nanosuspensions exhibit different polycrystalline peaks of the anatase TiO_2 phase. XRD measurements shown in Fig. 9 reveal that the peaks of the sintered nanoparticles are well-defined and match those obtained by Refs. 10, 14, 31, and 32. The crystalline planes for both sintered phases [anatase (blue data) and amorphous (red data)] of (101) at 25°, (112) at 37.7°, (200) at 48°, and (213) at 62°, are related to the anatase crystalline form of TiO_2, as reported previously in Refs. 31 and 32. In contrast, no crystalline peaks were observed that correspond to the rutile phase of TiO_2. This result agrees with the reported studies in which the transformation to the rutile phase can only occur above 600 °C.[13,15] The XRD peak localized at $2\theta = 25°$ (Fig. 9) proved that the sintered TiO_2 films preserved as the anatase TiO_2 phase.[31,33]

Spectrophotometry measurement from UV to IR region was carried out by measuring the transmittance. Shown in Fig. 10 is the optical transmittance of the wet and sintered anatase TiO_2 films. The transmittance increased nearly linearly over the UV to visible range and reached a maximum of ~91% in the IR region (~2550 nm). The transmittance of the wet TiO_2 film (Fig. 10) follows the same increment and reaches a maximum of 87% at 2550 nm. The sintered TiO_2 film shows an enhancement in transmittance from 87% to 91%. When the TiO_2 nanoparticles are sintered by a 10.6 μm laser, as the laser absorptivity is low, only a fraction of the laser energy can be absorbed by the top layer of the deposited TiO_2 patterns. Hence, CO_2 laser can penetrate through the entire titania film, which leads to uniform sintering of nanoparticles and high optical transparency.

For the spectrophotometry measurement of the sintered amorphous TiO_2 film, a transmittance of 80% was achieved at 2500 nm (Fig. 11). The image of the sintered amorphous TiO_2 film is shown as an inset in Fig. 11. The results demonstrate that it is possible to print transparent TiO_2 films using pure anatase TiO_2 nanosuspensions for application in advanced optics; e.g., for coating optical lenses.

Figure 12 shows the "average size of sintered grain," which represents the size of TiO_2 grains between the cracks, not the conventional grain size caused by the crystallization of materials. Bonding of TiO_2 NPs occurs at the threshold laser power 2 W, and cracks appear for sintering at high powers 3.55 and 3.95 W. For the grain size obtained at 1.1 W in the evaporation step, the average size of a sintered grain (Table III) is determined by calculating the average of several measured distances between two consecutive cracks after the evaporation of EG. The sintering at higher powers caused weak bonding between the NPs, resulting in the

removal of material. Also, we assumed that the sintered patterns at ~2 W can be considered as a single piece, crack-free line without any removal of TiO_2 material. It is observed (Fig. 12) that the average grain size decreases when the power is increased. This is due to the removal of material and also the shrinkage caused by micro-cracks on the printed TiO_2 patterns.

The number of sintered TiO_2 grains per mm^2 increases when the laser power increases (Table III). At 2 W, the size of the sintered grain tends to be the size of the whole sintered area, and the number of sintered TiO_2 grains per mm^2 tends to ~0, as shown in Fig. 12. A crack-free deposition can be obtained by minimizing the sintering laser power to 2 W.

Figure 13 summarizes the measured transmittance for different thin TiO_2 films deposited on glass and quartz substrates using both anatase and amorphous TiO_2 nanosuspensions.

V. CONCLUSIONS

In summary, we have demonstrated a novel technique based on the NELD process for manufacturing transparent inorganic glasses with sufficient quality and high transmittance for application in advanced optics. The NELD technique is considered as a novel promising technology because of the ability to reduce cross contamination, enable precise localized heating (micro-sintering), and versatility to sinter TiO_2 nanoparticles. The borosilicate glass substrate was found to break due to thermal stress because of the high heating rate. This issue was mitigated by developing a heat transfer model to obtain used laser dose as a function of temperature around the vicinity of the micro-focused laser spot. This model allowed the choice of proper processing parameters and minimized the number of experiments. XRD analysis pointed out that the crystalline anatase properties were preserved after laser treatment, eliminating the presence of the rutile phase. The obtained high transmittance of TiO_2 films in this study can find applications in advanced optics. Finally, we anticipate that the NELD technology will find a broad range of applications for the additive manufacturing of different functional microdevices.

ACKNOWLEDGMENTS

This work was supported by Naval Air Warfare Center Aircraft Division, IRflex Corporation under Contract No. N6893621C0039 and the Postdoctoral Scholar Program of UCF (P3 Program) under Contract No. 65019B31. The authors thank A. R. Regmi and appreciate the Materials Characterization Facility and the CREOL cleanroom at UCF.

AUTHOR DECLARATIONS

Conflict of Interest

The authors have no conflicts to disclose.

Author Contributions

Yahya Bougdid: Conceptualization (equal); Formal analysis (equal); Methodology (equal); Software (equal); Visualization (equal); Writing – original draft (equal). **Francois Chenard:** Funding acquisition (equal); Project administration (equal); Writing – review & editing (equal). **John Sugrim:** Funding acquisition (equal); Project administration (equal); Writing – review & editing (equal). **Ranganathan Kumar:** Conceptualization (equal); Formal analysis (equal); Funding acquisition (equal); Investigation (equal); Methodology (equal); Project administration (equal); Resources (equal); Supervision (equal); Writing – review & editing (equal). **Aravinda Kar:** Conceptualization (equal); Formal analysis (equal); Investigation (equal); Methodology (equal); Resources (equal); Supervision (equal); Validation (equal); Writing – review & editing (equal).

REFERENCES

[1]O. E. Castillo, R. Kumar, and A. Kar, "Laser electrospray printing of nanoparticles on flexible and rigid substrates," J. Laser Appl. **31**, 022015 (2019).
[2]Y. Liu, N. Peng, Y. Yao, X. Zhang, X. Peng, L. Zhao, J. Wang, L. Peng, Z. Wang, K. Mochizuki, M. Yue, and S. Yang, "Breaking the nanoparticle's dispersible limit via rotatable surface ligands," Nat. Commun. **13**, 3581 (2022).
[3]T. Li, A. Kar, and R. Kumar, "Marangoni circulation by UV light modulation on sessile drop for particle agglomeration," J. Fluid Mech. **873**, 72–88 (2019).
[4]T. Li, A. Kar, and R. Kumar, "Concentration distribution of photosensitive liquid in a droplet under ultraviolet light," J. Fluids Eng. **142**, 021301 (2019).
[5]T. Li, A. Kar, and R. Kumar, "Uniform and Gaussian ultraviolet light intensity distribution on droplet for selective area deposition of particles," J. Fluids Eng. **142**, 094503 (2020).
[6]J. F. Mousumi, G. Gregory, J. P. Ganesan, C. Nunez, K. Provancha, S. Seren, H. Zunft, T. Jurca, P. Banerjee, A. Kar, R. Kumar, and K. O. Davis, "Process-structure-properties relationships of passivating, electron-selective contacts formed by atmospheric pressure chemical vapor deposition of phosphorus-doped polysilicon," Phys. Status Solidi RRL **16**, 2100639 (2022).
[7]P. Pathak, O. E. Castillo, R. Kumar, A. Kar, and H. J. Cho, "Effect of laser power on conductivity and morphology of silver nanoparticle thin films prepared by a laser assisted electrospray deposition method," J. Laser Appl. **33**, 012034 (2021).
[8]H. Yang, W. Liu, C. Xu, D. Fan, Y. Cao, and W. Xue, "Laser sintering of TiO_2 films for flexible dye-sensitized solar cells," Appl. Sci. **9**, 823 (2019).
[9]H. Takikawa, T. Matsui, T. Sakakibara, A. Bendavid, and P. J. Martin, "Properties of titanium oxide film prepared by reactive cathodic vacuum arc deposition," Thin Solid Films **348**, 145–151 (1999).
[10]H. P. Fathi, H. Johnson, Z. Ahmadi, M. Roach, N. Shamsaei, and S. M. Mahjouri, "Laser-assisted selective and localized surface transformation of titanium to anatase, rutile, and mixed phase nanostructures," J. Laser Appl. **33**, 012014 (2021).
[11]S. Dutta, A. K. Patra, S. De, A. Bhaumik, and B. Saha, "Self-assembled TiO_2 nanospheres by using a biopolymer as a template and its optoelectronic application," ACS Appl. Mater. Interfaces **4**, 1560–1564 (2012).
[12]J. Yu, X. Zhao, and Q. Zhao, "Photocatalytic activity of nanometer TiO_2 thin films prepared by the sol-gel method," Mater. Chem. Phys. **69**, 25–29 (2001).
[13]J.-X. Liu, D.-Z. Yang, F. Shi, and Y.-J. Cai, "Sol–gel deposited TiO_2 film on NiTi surgical alloy for biocompatibility improvement," Thin Solid Films **429**, 225–230 (2003).
[14]N. R. Mathews, E. R. Morales, J. M. Cortés, and A. J. Toledo, "Tio_2 thin films: Influence of annealing temperature on structural, optical, and photocatalytic properties," Solar Energy **83**, 1499–1508 (2009).
[15]V. J. Nagpal, R. M. Davis, and S. B. Desu, "Novel thin films of titanium dioxide particles synthesized by a sol-gel process," J. Mater. Res. **10**, 3068–3078 (1995).
[16]L. Schade, S. Franzka, S. Hardt, H. Wiggers, and N. Hartmann, "Sintering of thin titanium dioxide nanoparticle films via photothermal processing with ultraviolet continuous-wave lasers," Appl. Surf. Sci. **278**, 336–340 (2013).
[17]O. E. Castillo, R. Kumar, and A. Kar, "Thermal response of Bessel beam-heated microdroplets carrying nanoparticles for deposition," J. Laser Appl. **33**, 012043 (2021).

[18]O. E. Castillo, R. Kumar, and A. Kar, "Laser-induced subwavelength structures by microdroplet superlens," Opt. Express **27**, 8130–8142 (2019).
[19]T. Li, R. Kumar, and A. Kar, "Enhanced heating by microdroplet lens in nanoparticle electrospray laser deposition," J. Laser Appl. **33**, 012012 (2021).
[20]T. Li, K. O. Davis, R. Kumar, and A. Kar, "Diffraction and thermal effect of a Bessel-Gaussian laser for Ag nanoparticle deposition," Opt. Express **30**, 19246–19272 (2022).
[21]T. Li, A. Kar, and R. Kumar, "Volumetric laser heating of nanosuspension microdroplets: Slow evaporation to mid-air explosion," Int. J. Heat Mass Transfer **177**, 121433 (2021).
[22]Y. Bougdid, I. Maouli, A. Rahmouni, K. Mochizuki, I. Bennani, M. Halim, and Z. Sekkat, "Systematic resolution achieved in nanofabrication by two-photon-absorption induced polymerization," J. Micromech. Microeng. **29**, 035018 (2019).
[23]Y. Bougdid and Z. Sekkat, "Voxels optimization in 3D laser nanoprinting," Sci. Rep. **10**, 1–8 (2020).
[24]E. Sani and A. Dell'Oro, "Optical constants of ethylene glycol over an extremely wide spectral range," Opt. Mater. **37**, 36–41 (2014).
[25]F. P. Incropera and D. P. DeWitt, *Fundamentals of Heat and Mass Transfer*, 2nd ed. (Wiley and Sons, New York, 1985), p. 203.
[26]A. M. Prokhorov, V. I. Konov, I. Ursu, and I. N. Mihailescu, *Laser Heating of Metals*, English Edition (IOP, New York, 1990), p. 43.
[27]N. Mufti, I. K. R. Laila, Hartatiek, and A. Fuad, "The effect of TiO_2 thin film thickness on self-cleaning glass properties," IOP Conf.: Ser. J. Phys. Conf. Ser. **853**, 012035 (2017).
[28]M. Radovic, G. Dubourg, S. Kojic, M. Z. Dohčevic, B. Stojadinovic, M. Bokorov, and B. V. Crnojevic, "Laser sintering of screen-printed TiO_2 nanoparticles for improvement of mechanical and electrical properties," Ceram. Int. **44**, 10975–10983 (2018).
[29]W. Peng, W. Zeng, Y. Zhang, C. Shi, B. Quan, and J. Wu, "The effect of colored titanium oxides on the color change on the surface of Ti-5Al-5Mo-5V-1Cr-1Fe alloy," J. Mater. Eng. Perform. **22**, 2588–2593 (2013).
[30]J. Sun, Z. Xu, W. Li, and X. Shen, "Effect of nano-SiO_2 on the early hydration of alite-sulphoaluminate cement," Nanomaterials **7**, 102 (2017).
[31]M. Ghadiry, M. Gholami, C. K. Lai, H. Ahmad, and W. Y. Chong, "Ultra-sensitive humidity sensor based on optical properties of graphene oxide and nano-anatase TiO_2," PLoS One **11**, e0153949 (2016).
[32]D. Wojcieszak, M. Mazur, D. Kaczmarek, A. Poniedziałek, P. Domanowski, B. Szponar, A. Czajkowska, and A. Gamian, "Effect of the structure on biological and photocatalytic activity of transparent titania thin-film coatings," Mater. Sci.-Pol. **34**, 856–862 (2016).
[33]M. K. Hossain, M. F. Pervez, M. J. Uddin, S. Tayyaba, M. N. H. Mia, M. S. Bashar, M. K. H. Jewel, M. A. S. Haque, M. A. Hakim, and M. A. Khan, "Influence of natural dye adsorption on the structural, morphological, and optical properties of TiO_2 based photoanode of dye-sensitized solar cell," Mater. Sci.-Pol. **36**, 93–101 (2017).